Geochemistry, Geophysics, Geosystems

Supporting Information for

Accessory Mineral Eu Anomalies in Suprasolidus Rocks: Beyond Feldspar

R. M. Holder[1,2], C. Yakymchuk[3], and D. R. Viete[2]

[1]Department of Earth and Environmental Sciences, University of Michigan, Ann Arbor, Michigan, USA.

[2]Department of Earth and Planetary Sciences, Johns Hopkins University, Baltimore, MD, USA.

[3]Department of Earth and Environmental Sciences, University of Waterloo, Waterloo, ON, Canada.

Contents of this file

Additional Supporting Information (Files uploaded separately)

Data Sets S1 to S16

Introduction

This supporting information file contains Text S1, which provides additional information on the partitioning data used in the B94 models, and Text S2, which provides additional information on the partitioning data used in the MC models. The results of all models are tabulated in Tables S1 to S16, which are presented in a separate .xlsx file.

Text S1. Partition coefficients for the B94 models

These models use the empirical weight fraction partition coefficients estimated by Bea et al. (1994). Bea et al. (1994) measured the trace-element compositions of coexisting biotite, cordierite, garnet, monazite, zircon, apatite, alkali-feldspar, and plagioclase in peraluminous migmatites from the Peña Negra Complex, Spain, by LA-ICP-MS. Minerals in our models that were not included in the study of Bea et al. (1994) are muscovite, magnetite–spinel, ilmenite, quartz, and rutile. For muscovite we assumed that K_d^{REE} = biotite K_d^{REE}. Quartz and oxides were assumed not to incorporate REE. Values of K_d^{Eu3+} were determined as the geometric means of K_d^{Sm} and K_d^{Gd} in accordance with the predictable behavior of trivalent REE due to lanthanide contraction (e.g. Philpotts, 1970). Values of K_d^{Eu2+} were taken to equal K_d^{Sr}, due to the near-identical ionic radii of Sr^{2+} and Eu^{2+} (Shannon, 1976; Philpotts, 1970). Bea et al. (1994) did not report Sr concentrations in the accessory minerals and therefore K_d^{Eu2+}=0; a range of plausible K_d^{Eu2+} (< 0.1) were tested and found not to influence the results significantly due to the very low modes of these minerals and their strong preference for Eu^{3+} relative to Eu^{2+}. The advantages of the B94 models are that: (1) The estimated peak metamorphic temperature of the rocks from which the partitioning data were estimated (750°C) is lower than the experimental/magmatic temperatures of most trace-element partitioning studies and (2) The rocks from which the data were estimated are similar to the modeled compositions of this study (i.e. peraluminous migmatites). The B94 models do not account for the temperature- or pressure-dependence of partitioning.

Text S2. Partition coefficients for the MC models

These models use temperature-dependent partition coefficients from various studies. Equations for Sm, Eu^{2+}, Eu^{3+}, and Gd were used for plagioclase, alkali-feldspar, garnet, zircon, monazite, and apatite. Insufficient K_d^{REE} data are available for biotite, muscovite,

magnetite, ilmenite, rutile, or quartz. However, as discussed above, these minerals play little role in the overall REE budget compared to the other modeled phases; they are assumed not to incorporate REE in these models, for simplicity. The advantages of the MC models are that they account for the temperature dependence of partitioning and include both Eu^{2+} and Eu^{3+} in each accessory mineral.

Zircon and garnet: For Sm and Gd, zircon and garnet partitioning equations of the form $\log_{10}K_d = a/T+b$ were regressed from the combined results of Rubatto et al. (2007) and Taylor et al. (2015); a and b are constants and T is in K. All experiments from Rubatto et al. (2007) and Taylor et al. (2015) showed distinct Eu anomalies, suggesting the presence of both Eu^{2+} and Eu^{3+}. To circumvent this, K_d^{Eu3+} was regressed from the lattice-strain parameterization of Taylor et al. (2015; which uses ionic radius and therefore allows calculation of K_d^{Eu3+}, despite it not being measured) and the geometric means of K_d^{Sm} and K_d^{Gd} in the experiments of Rubatto et al. (2007). It was assumed that $K_d^{Eu2+} = K_d^{Sr}$. Garnet K_d^{Sr} has been estimated primarily for garnet:basalt systems and has generally been estimated to be <0.01 (GERM database). A single garnet K_d^{Sr} value from a rhyolite, which is likely more appropriate for the modeled systems of this study, was estimated to be 0.02 at T~1000°C (Sisson and Bacon, 1992). Therefore, an equation for garnet K_d^{Eu2+} of the form $\log_{10}K_d = a/T+b$ was calculated such that K_d^{Eu2+}=0.02 at 1000°C; the temperature-dependence (coefficient a) was assumed to be identical to garnet K_d^{Eu3+}. Zircon is not commonly considered to have Sr or Eu^{2+} as impurities. To our knowledge, there are no data for zircon K_d^{Eu2+} or K_d^{Sr}, although zircon:whole-rock Sr ratios of ~ 0.001 have been measured in intermediate igneous rocks and might provide an approximate value (Ballard et al., 2002). Zircon:garnet Eu ratios generally vary near unity (Rubatto and Hermann, 2007; Taylor et al., 2015). Therefore, for consistency between zircon and garnet, we treated zircon K_d^{Eu2+} the same as garnet K_d^{Eu2+}. We assumed it to have a value of 0.02 at 1000°C and a temperature dependence identical to zircon K_d^{Eu3+}.

Monazite: partitioning equations were calculated for Sm, Eu^{3+}, and Gd in monazite from the experiments of Stepanov et al. (2012). The experiments of Stepanov et al. (2012) were conducted over a range of temperatures, pressures, and water

contents. Although each of these variables was found to influence monazite:melt partitioning, the dominant control was found to be temperature. Because the full relationships among pressure, water content, and monazite partitioning coefficients remains somewhat ambiguous, the monazite partitioning equations used in this study were calculated by regressions of all experimental partitioning data of Stepanov et al. (2012: all pressures and H_2O contents) against temperature following the same functional form used for garnet and zircon: $\log_{10}D = a/T+b$. As with the zircon–garnet–melt experiments (Rubatto et al., 2007; Taylor et al., 2015), the monazite–melt experiments of Stepanov et al. (2012) show distinct Eu anomalies suggestive of both Eu^{3+} and Eu^{2+}. Therefore, K_d^{Eu3+} was calculated as the geometric mean of K_d^{Sm} and K_d^{Gd}. In preliminary calculations, the concentrations of Sm, Eu, and Gd in monazite and garnet:monazite K_d^{REE} were lower observed in natural samples (e.g. Hermann and Rubatto, 2003; Buick et al., 2006; Rubatto et al., 2006; Mottram et al., 2014; Warren et al., 2019; Hacker et al., 2019). Monazite K_d^{REE} were therefore multiplied by 50 to provide better agreement with natural samples (monazite:garnet Gd and Eu ratios of a few 1000). Monazite K_d^{Eu2+} was estimated from Sr data. Stepanov et al. (2012) reported a single measurement of Sr in monazite and melt from their experiment C3970, conducted at 1000°C: 21 ppm Sr in monazite and 59 ppm in the melt, corresponding to $K_d^{Sr,Eu2+} = 0.35$. As with garnet and zircon, monazite K_d^{Eu2+} was made to pass through this point and given the same temperature dependence as monazite K_d^{Eu3+}.

Apatite: partitioning equations for Sm, Eu, and Gd in apatite were calculated from the experiments of Watson and Green (1981). Watson and Green (1981) measured apatite partitioning as a function of melt composition and temperature. Because the melts of this study are most similar to their experimental granites, apatite partitioning equations of the form $\log_{10}D = a/T+b$ were calculated using only those experiments. For apatite K_d^{Sm}, we used their experimental data directly. For apatite K_d^{Eu2+}, we used their experimental data for Sr. For apatite K_d^{Eu3+} and K_d^{Gd} (neither measured), we used the geometric mean of K_d^{Sm} and K_d^{Dy} in recognition that apatite K_d^{MREE} are approximately equal. Although Watson and Green (1981) only conducted two experiments with granitic

melts, they express confidence that their results should extrapolate well to lower and higher temperatures based on systematic observations of their dataset for a range of melt compositions.

Plagioclase: Plagioclase K_d^{Eu2+} was taken from the lattice-strain model of Sun et al. (2017), which is a function of temperature, pressure, and plagioclase composition. Although this lattice-strain model was calibrated for plagioclase–basalt systems, it has been shown that temperature and plagioclase composition play a much larger role in K_d^{Sr} (and therefore K_d^{Eu2+}) than melt/fluid/rock composition (Blundy and Wood, 1991) and therefore the calibration was deemed reasonable for this study. For the modeled *P–T* range, plagioclase K_d^{Eu2+} was calculated to be 1.1–9 in the pelite models and 4.5–14 in the greywacke models, broadly consistent with expectations that this value be greater than unity, but not by multiple orders of magnitude. Plagioclase K_d^{Eu3+} was also initially calculated with the lattice-strain model of Sun et al. (2017), however this resulted in values that were consistently and unreasonably low for the model conditions (<<0.01); therefore, plagioclase K_d^{Eu3+} was set to equal $0.1 \bullet K_d^{Eu2+}$. This maintains a consistently large positive Eu anomaly for the model plagioclase, consistent with natural observations.

Alkali-feldspar: Alkali-feldspar K_d^{Eu2+} was modeled using the composition-only K_d^{Sr} equation of Ren (2004). The model values of alkali-feldspar K_d^{Eu2+} were calculated to be ~6–15 in both pelite and greywacke models, comparable to the values for plagioclase. Initially, we also took alkali-feldspar K_d^{Eu3+} from Ren (2004; interpolated from K_d^{Ce}, K_d^{Nd}, and K_d^{Yb}); however, these expressions were calibrated explicitly as functions of whole-rock SiO_2 and Al_2O_3 and were found not to extrapolate well beyond the rhyolite-compositions investigated by Ren (2004). Therefore, the same approach was taken as with plagioclase. Alkali-feldspar K_d^{Eu3+} was set to equal $0.1 \bullet K_d^{Eu2+}$, maintaining consistent positive Eu anomalies for alkali-feldspar in the models.

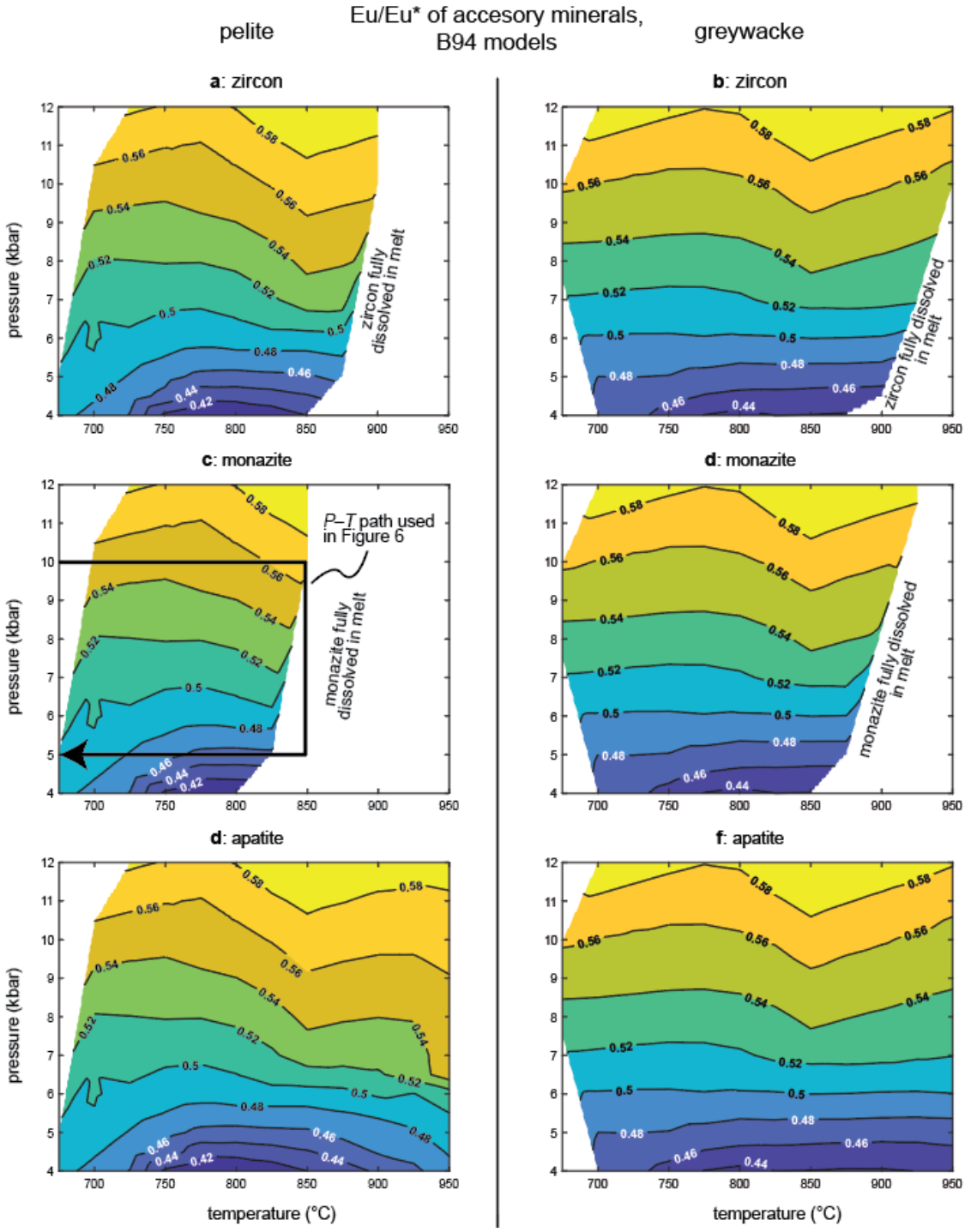

Figure S1. Eu anomalies from the B94 models. (a,b) Zircon; (c,d) Monazite; (e,f) Apatite.

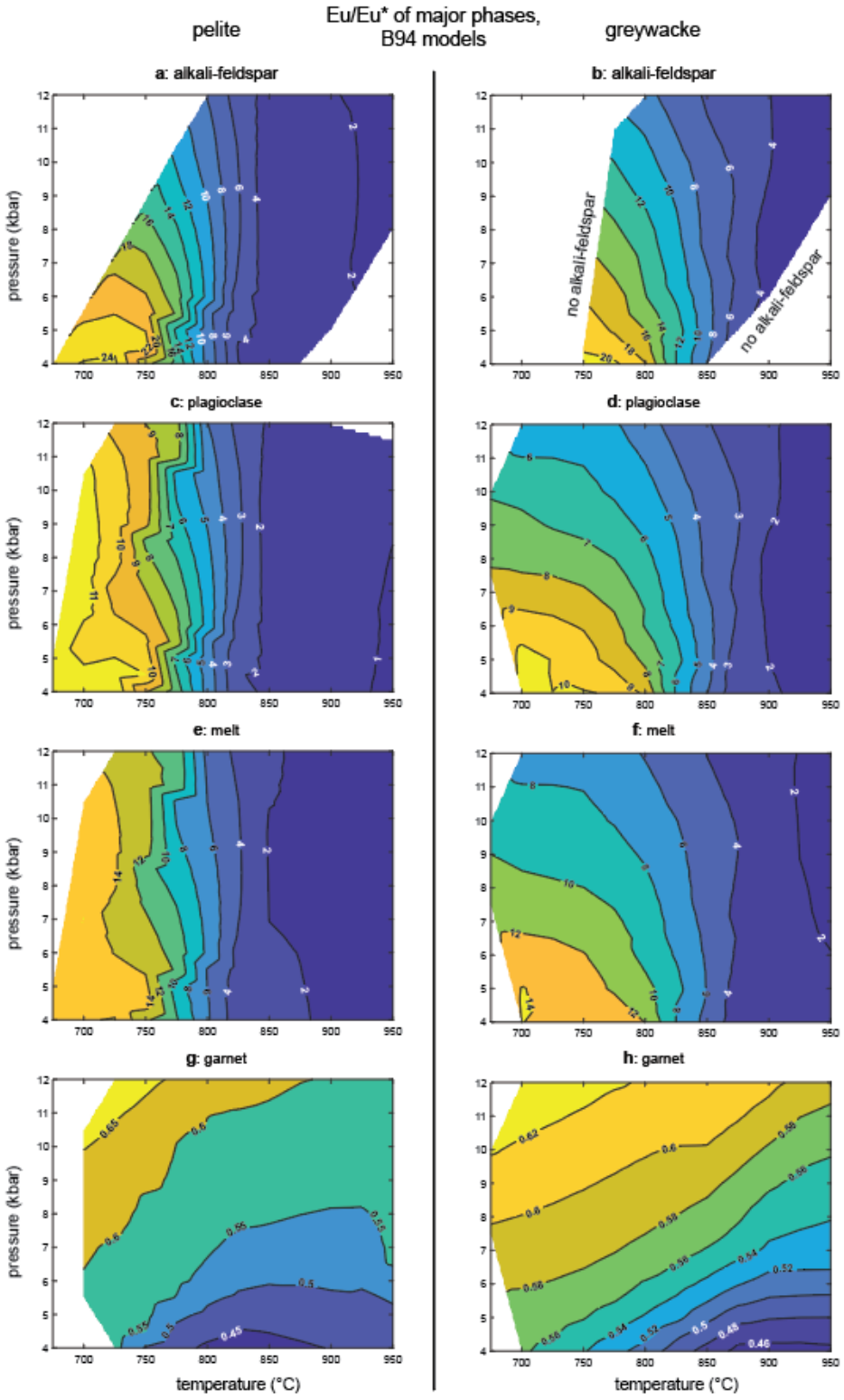

Figure S2. Eu anomalies from the B94 models. (a,b) Alkali-feldspar; (c,d) Plagioclase; (e,f) Melt; (g,h) Garnet.

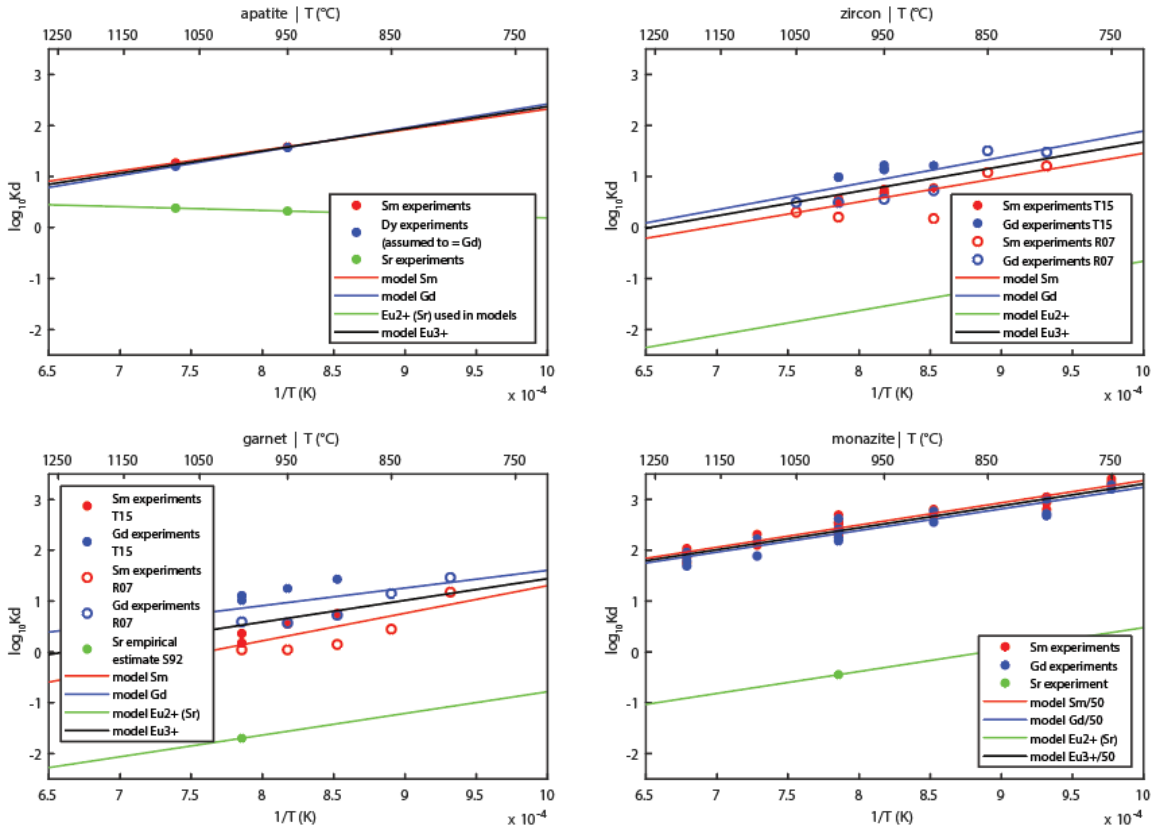

Figure S3. Temperature-dependent partitioning data for accessory minerals and garnet, used in the MC models. Apatite data from Watson and Green (1981). Zircon and garnet data from: R07, Rubatto and Hermann (2007); T15, Taylor et al. (2015); S92, Sisson and Bacon (1992). Monazite data from Stepanov et al. (2012).

Data Set S1. Equilbrium pelite partitioning model using the MC partitioning dataset.

Data Set S2. Pressure-temperature path extracted from the equilbrium pelite model using the MC partitioning dataset.

Data Set S3. Equilbrium pelite partitioning model using the B94 partitioning dataset.

Data Set S4. Pressure-temperature path extracted from the equilbrium pelite model using the B94 partitioning dataset.

Data Set S5. Equilbrium greywacke partitioning model using the MC partitioning dataset.

Data Set S6. Pressure-temperature path extracted from the equilbrium greywacke model using the MC partitioning dataset.

Data Set S7. Equilbrium greywacke partitioning model using the B94 partitioning dataset.

Data Set S8. Pressure-temperature path extracted from the equilbrium greywacke model using the B94 partitioning dataset.

Data Set S9. Pelite partitioning model with feldspar fractionation using the MC partitioning dataset.

Data Set S10. Pelite partitioning model with feldspar fractionation using the B94 partitioning dataset.

Data Set S11. Greywacke partitioning model with feldspar fractionation using the MC partitioning dataset.

Data Set S12. Greywacke partitioning model with feldspar fractionation using the B94 partitioning dataset.

Data Set S13. Pelite partitioning model with melt extraction using the MC partitioning dataset.

Data Set S14. Pelite partitioning model with melt extraction using the B94 partitioning dataset.

Data Set S15. Greywacke partitioning model with melt extraction using the MC partitioning dataset.

Data Set S16. Greywacke partitioning model with melt extraction using the B94 partitioning dataset.